Stereochemistry of Boron-Functionalized (Dioximato)iron(II) Complexes. Control of Nonbonded Interactions on Soft Conformational Surfaces

Isak Vernik and Dennis V. Stynes*

Department of Chemistry, York University, North York, Ontario, Canada M3J 1P3

Received March 13, 1996[⊗]

The structural and energetic consequences of nonbonded interactions between axial ligands and minimally superstructured borylated iron bis(dioxime) complexes are described. Structural data for 20 low spin axially ligated derivatives are compared. Complexes of $Fe((DMG)BPh_2)_2(Py)L$, L = NH_3, TCNE, $PMePh_2$, and Py and $Fe((DMG)BF_2)_2L_2$, L = Py, and 4-*t*-BuPy, crystallize in the C_{2v} conformation. The complexes, $Fe((DMG)BPh_2)_2L_2$, L = CH_3CN, $CH_3CH_2CH_2CN$, $BuNH_2$, *i*-$PrNH_2$, and piperidine (PIP), and an Fe(III) derivative, $[Et_4N][Fe((DMG)BF_2)_2(Cl)_2]$, all adopt the centrosymmetric C_{2h} conformation. The cyclophane-like binding cavity in the C_{2v} complexes of $Fe((DMG)BPh_2)_2$ opens or closes in response to attractive or repulsive interactions between the cavity and axial ligands. Face strain effects are largely responsible for the binding order $BuNH_2$ > *i*-$PrNH_2$ > PIP and 1−MeIm > Py in $Fe((DMG)BR_2)_2L_2$ complexes. They favor the exceptional C_{2v} conformer for bis(pyridine) complexes, enforce an eclipsed conformation about the N−C_α bond of *i*-$PrNH_2$, and cause a 0.12 Å bond lengthening for PIP. The orientation of axial ligands in FeN_4 systems is controlled via the combined effects of axial interactions and face strain. Steric and Coulombic forces have a significant effect on binding energetics but London forces do not. Strategies for the effective use of nonbonded interactions in conformationally complex systems are described.

Introduction

A single multidimensional free energy surface serves to define the structure, conformation, and thermodynamic and kinetic stabilities of complex molecular systems. Both bonded and nonbonded interactions contribute to the energetics of this surface. The latter, while simple in concept, prove to be the most difficult to organize and control. Nonbonded interactions are primarily responsible for the functional properties of biochemical systems, and their manipulation is critical to biomimetic studies.

Borylated bis(dioximato)iron complexes[1] provide a simple way of positioning groups in close proximity to iron bound ligands without incurring some of the difficulties[2] encountered with more elaborately superstructured heme and related systems.[3] The energetics associated with axial nonbonded interactions have been quantified on the basis of ligand binding differences between the closely related $Fe((DMG)BPh_2)_2$ and $Fe((DMG)BF_2)_2$ systems, and some impressive effects have been demonstrated.[1c]

Two conformations of $Fe((DMG)BR_2)_2$ complexes (see Figure 1) arise related by facile flips of the boroximatoiron chelate rings. The C_{2v} conformation has been structurally characterized in carbonyl derivatives[1d] ($Fe((DMG)BR_2)_2(Py)(CO)$, BR_2 = BPh_2 , BF_2 and BBN) and in two μ-oxo complexes[1e] $[Fe((DMG)BPh_2)_2]_2O$ and $[(BuNH_2)Fe((DMG)BPh_2)_2)]_2O$. The centrosymmetric C_{2h} conformer is found in the symmetrically substituted derivatives $Fe((DMG)BPh_2)_2(MeIm)_2$[1f] and $Fe((DMG)BR_2)_2(BuNH_2)_2$, BR_2 = BPh_2, BF_2 and BBN.[1d]

In this work we present crystallographic results for a baker's dozen of new complexes. These establish the structural features characteristic of the 14-membered bis(dioximatoborate) macrocycle in its two common conformations. We then examine the details of attractive and repulsive nonbonded contacts found in various ligated derivatives. When combined with extensive equilibria and rate measurements presented in earlier work, these data permit a definitive examination of structure/reactivity relationships and they provide a unique insight into the interplay between nonbonded interactions, conformation, and binding energetics in a minimally superstructured metal complex.

Experimental Section

Complexes were prepared and characterized as described previously.[1d] Crystals were grown from CH_2Cl_2/hexane via slow diffusion except as follows: **6**, slow evaporation of pyridine solution; **11** and **12**, slow evaporation of CH_2Cl_2/RCN.

Crystallography. Single-crystal X-ray data were collected at room temperature on a Siemens R3m/v diffractometer using graphite-monochromatized Mo Kα radiation (λ = 0.710 73 Å). Cell parameters were typically determined from 25−40 reflections. Three standard

[⊗] Abstract published in *Advance ACS Abstracts,* August 15, 1996.

(1) (a) Stynes, D. V.; Leznoff, D.; de Silva, D. G. A. H. *Inorg. Chem.* **1993**, *32*, 3989. (b) Impey, G.; Stynes, D. V. *J. Am. Chem. Soc.* **1993**, *115*, 7868. (c) Stynes, D. V. *Inorg. Chem.* **1994**, *33*, 5022. (d) de Silva, D. G. A. H.; Leznoff, D.; Impey, G.; Vernik, I.; Jin, Z.; Stynes, D. V. *Inorg. Chem.* **1995**, *34*, 4015. (e) Vernik, I.; Stynes, D. V. *Inorg. Chem.* **1996**, *35*, 2006. (f) Jansen, J. C.; Verhage, M. *Cryst. Struct. Commun.* **1982**, *11*, 305. (g) Vernik, I.; Stynes, D. V. *Inorg. Chem.* **1996**, *35*, 2011. (h) Vernik, I.; Stynes, D. V. *Inorg. Chem.* **1996**, *35*, 1093.

(2) (a) Portela, C. F.; Magde, D.; Traylor, T. G. *Inorg. Chem.* **1993**, *32*, 1313. (b) David, S.; James, B. R.; Dolphin, D.; Traylor, T. G.; Lopez, M. A. *J. Am. Chem. Soc.* **1994**, *116*, 6. (c) Munro, O. Q.; Bradley, J. C.; Hancock, R. D.; Marques, H. M.; Marsicano, F.; Wade, P. G. *J. Am. Chem. Soc.* **1992**, *114*, 7218.

(3) (a) Hashimoto, T.; Dyer, R. L.; Crossley, M. J. Baldwin, J. E.; Basolo, F. *J. Am. Chem. Soc.* **1982**. *104*, 2101. (b) Kim, K.; Ibers, J. A. *J. Am. Chem. Soc.* **1991**, *113*, 6077. (c) Kim, K.; Fettinger, J.; Sessler, J. L.; Cyr, M.; Hugdahl, J.; Collman, J. P.; Ibers, J. A. *J. Am. Chem. Soc.* **1989**, *111*, 403. (d) Collman, J. P.; Brauman, J.; Fitzgerald, J. P. Hampton, P. D.; Naruta, Y. P.; Sparapany, J. W.; Ibers, J. I. *J. Am. Chem. Soc.* **1988**, *110*, 3477. (e) Collman, J. P.; Brauman, J. I.; Fitzgerald, J. P.; Sparapany, J. W.; Ibers, J. I. *J. Am. Chem. Soc.* **1988**, *110*, 3486. (f) Mandon, D.; Ott-Woelfel, F.; Fischer, J.; Bill, E.; Trautwein, A. X. *Inorg. Chem.* **1990**, *29*, 2442. (g) Traylor, T. G.; Tsuchiya, S.; Campbell, D.; Mitchell, M.; Stynes, D.; Koga, N. *J. Am. Chem. Soc.* **1985**, *107*, 604.

S0020-1669(96)00276-5 CCC: $12.00

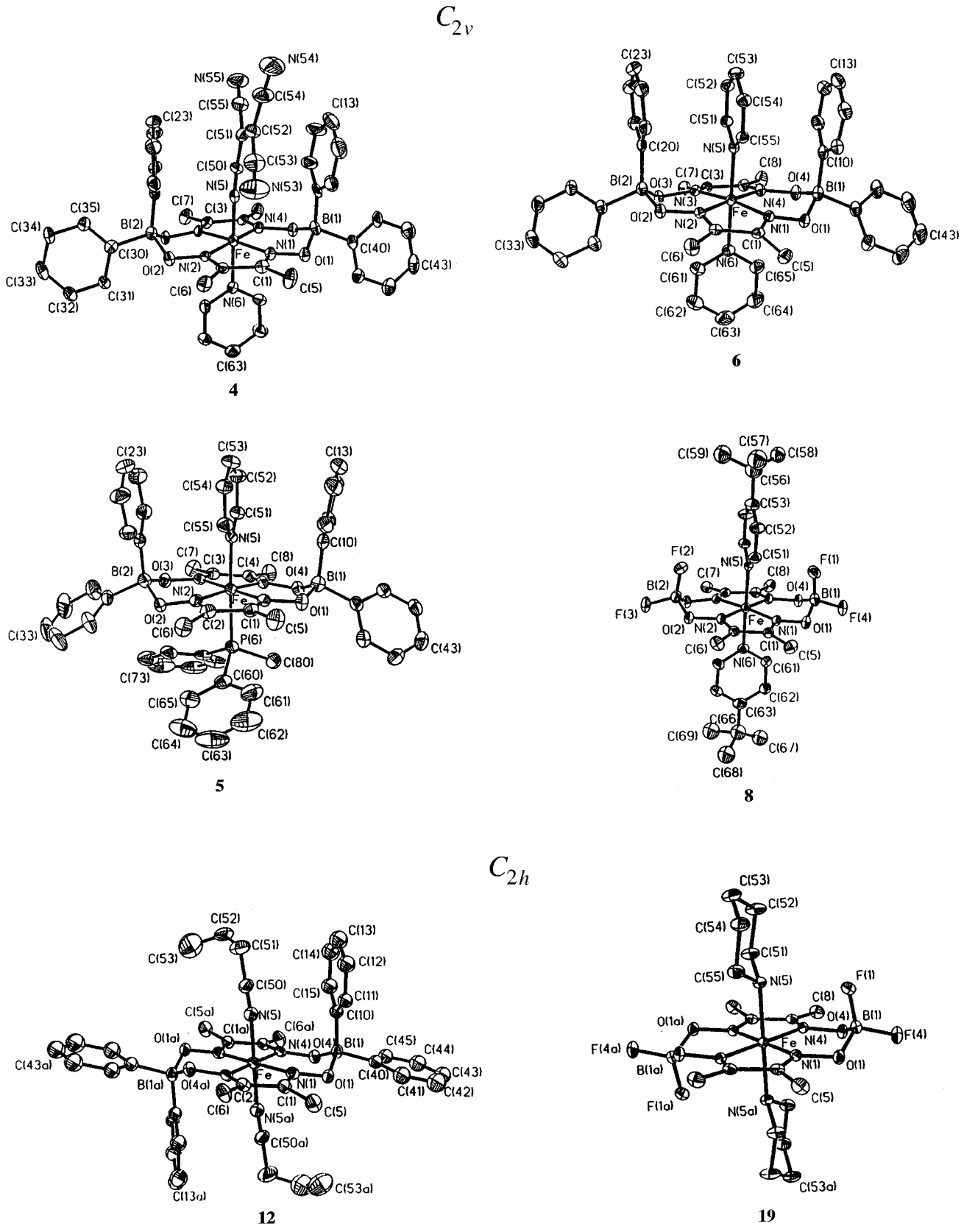

Figure 1. ORTEPs with 30% probability ellipsoids. Complexes **4**, **5**, **6**, and **8** adopt the C_{2v} conformation; complexes **12** and **19** adopt the centrosymmetric C_{2h} structure.

reflections were measured after every 97 reflections. Absorption corrections (XEMP) were typically applied on the basis of ψ scans. Structures were solved by direct or Patterson methods followed by Fourier syntheses. Final refinement was done by full-matrix least-squares procedures using anisotropic thermal parameters except as noted for **18**. Hydrogen atoms were placed in idealized positions (C−H 0.96 Å, N−H 0.90 Å) and refined isotropically ($U_{11} = 0.08$ Å^2) with a riding model. Structure solution used the SHELXTL PLUS (PC) package with final least-squares refinement on F^2 using SHELXL-93.[4] Crystallographic details are provided in the supporting information.

Table 1. Crystallographic Data Summary for $Fe((DMG)BPh_2)_2(L)(L')$ Complexes

	3	**4**	**5**	**6**	**11**	**12**
L	NH_3	TCNE	$PMePh_2$	Py	$\mathbf{CH_3}CN$	$\mathbf{C_3}H_7CN$
L′	Py	Py	Py	Py	CH_3CN	C_3H_7CN
fw	799.1	991.4	893.4	772.3	772.3	752.3
space group	*Pbcn*	$P2_1$	$P\bar{1}$	$P2_1/c$	$P\bar{1}$	$P2_1/c$
a, Å	15.002(3)	10.371(2)	11.499(5)	19.694(4)	8.641(1)	8.944(2)
b, Å	16.034(3)	19.599(4)	11.569(5)	11.762(2)	8.950(4)	11.348(2)
c, Å	16.251(3)	12.363(2)	20.087(8)	17.264(3)	14.277(2)	19.864(4)
α, deg	90	90	75.81	90	106.06	90
β, deg	90	109.56(3)	87.99	92.26(3)	103.71	101.11(3)
γ, deg	90	90	62.25(1)	90	97.38	90
V, Å^3	3909.0(13)	2367.9(8)	2283(2)	3995.9(13)	1008.3(5)	1978.3(7)
Z	4	2	2	4	1	2
μ, mm^{-1}	0.570	0.597	0.416	0.426	0.424	0.429
ρ, Mg/m^3	1.353	1.390	1.30	1.284	1.272	1.263
no. of indep reflcns	2318	3193	7864	7039	3525	3485
no. of params	247	537	568	496	250	186
GOF on F^2	1.08	0.93	1.11	1.03	1.05	0.76
max diff peak, e/Å^3	0.35	0.25	1.04	0.36	0.59	0.33
max diff hole, e/Å^3	−0.43	−0.22	−0.44	−0.31	−0.65	−0.32
R_1 ($I > 2\sigma$)	0.057	0.042	0.073	0.052	0.068	0.065
wR2 (F^2)	0.140	0.084	0.17	0.11	0.19	0.12

Table 2. Crystallographic Data Summary for $Fe((DMG)BR_2)_2L_2$ Complexes

	7	**8**	**16**	**17**	**19**	**20**
R	F	F	Ph	F	F	F
L	Py	4-*t*-BuPy	*i*-$PrNH_2$	*i*-$PrNH_2$	PIP	Cl
fw	539.89	821.05	902.16	499.91	551.98	582.84
space group	$P2_12_12_1$	$P2_12_12_1$	$P\bar{1}$	$P\bar{1}$	$P2_1/n$	$P\bar{1}$
a, Å	10.533(5)	12.839(1)	10.313(3)	9.688(2)	8.531(1)	7.811(2)
b, Å	13.171(4)	12.843(2)	10.597(2)	10.464(1)	11.974(2)	8.045(2)
c, Å	17.059(6)	23.545(2)	11.376(4)	11.823(1)	12.067(1)	11.748(2)
α	90	90	84.72	89.97(1)	90	76.53(3)
β	90	90	67.78	79.21(1)	97.29(1)	73.10(3)
γ	90	90	89.97	72.23(1)	90	63.04(3)
V, Å^3	2367(2)	3882.4(8)	1145.2(6)	1119.1(3)	1222.7(3)	625.1(2)
Z	4	4	1	2	2	1
μ, mm^{-1}	0.706	0.583	0.607	0.739	0.685	0.879
ρ, Mg/m^3	1.515	1.285	1.308	1.483	1.499	1.548
no. of reflcns	2885	4522	2789	6532	3557	2084
no. of params	316	426	259	312	164	175
GOF (F^2)	1.063	0.804	1.018	1.063	1.023	1.085
max diff peak, e/Å^3	0.33	0.48	0.326	0.532	0.439	0.873
max diff hole, e/Å^3	−0.29	−0.63	−0.337	−0.465	−0.456	−0.399
R_1 ($I > 2\sigma$)	0.056	0.059	0.082	0.040	0.043	0.044
wR2 (F^2)	0.083	0.16	0.144	0.108	0.105	0.12

Results

Crystallographic data for new structures are collected in Tables 1 and 2 and additional details are provided in the supporting material. Structural data for complexes displaying the C_{2v} conformation are given in Table 3. Data for those displaying the C_{2h} geometry are assembled in Table 4. Figure 1 displays the ORTEPs for selected examples of the two conformations in the BF_2 and BPh_2 systems.

Results for the new structures are described below along with a brief description of some previously reported structures. Ten adopt the C_{2v} conformation (**1**−**10**), and ten adopt the centrosymmetric C_{2h} geometry (**11**−**20**). Two types of nonbonded interaction are noted. Axial interactions refer to contacts between the axial ligand and axial B−Ph or B−F groups. Face strain[5] refers to nonbonded repulsions associated with contacts between α-CH groups of the axial ligands (especially for pyridine, piperidine, and isopropylamine ligands) and the face of the tetradentate planar macrocycle. These forces combine to alter the conformational and binding energetics and they also serve to determine the favored orientation of the bound ligand. Diagrams showing the orientation of axial pyridine and imidazole ligands in several borylated complexes are shown in Figure 2 along with the classic unborylated $Fe(DMGH)_2(Im)_2$ (**21**) structure reported by Bowman.[6a]

The orientation of the axial ligands with respect to the tetradentate ligand is defined in terms of the dihedral angle, ϕ, formed between a plane defined by the pairs of axial donor and boron atoms and the axial ligand plane. The angle ϕ differs slightly from the corresponding definition for hemes,[7] where $\phi = 0°$ corresponds to an Fe−N bond vector. In the lower symmetry dioxime complexes, a radial vector in the N_4 plane intersects projections of the B, O, N, and C atoms of the macrocycle at 0, 26, 48, and 75° respectively. The bisector of the diimine chelate rings lies at $\phi = 90°$.

(4) (a) Sheldrick, G. M. SHELXTL PC version 4.1. Siemens Analytical X-Ray Instruments Inc. Madison, WI. (b) Sheldrick, G. M. SHELXL-93. Gottingen, Germany.

(5) (a) Geibel, L.; Cannon, J.; Campbell, D.; Traylor, T. G. *J. Am. Chem. Soc.* **1978**, *100*, 3575. (b) Radonovich, L. J.; Bloom, A.; Hoard, J. L. *J. Am. Chem. Soc.* **1972**, *94*, 2073.

(6) (a) Bowman, K.; Gaughan , A. P.; Dori, Z. *J. Am. Chem. Soc.* **1972**, *94*, 727. (b) Prout, C. K.; Wiseman, T. J. *J. Chem. Soc. A* **1964**, 497.

(7) (a) Scheidt, W. R.; Gouterman, M. in *Iron Porphyrins, Part I*; Addison Wesley: Reading, MA, Lever, A. B. P., Gray,H. B., Eds; 1983; pp 91−139. (b) Scheidt, W. R.; Reed, C. A. *Chem. Rev.* **1981**, *81*, 543. (c) Scheidt, W. R.; Lee, Y. J. *Struct. Bonding* **1987**, *64*, 1. (d) Collins, D. M.; Countryman, R.; Hoard, J. L. *J. Am. Chem. Soc.* **1972**, *94*, 2066.

Table 3. Structural Comparison of C_{2v} Fe((DMG)BR_2)$_2$LT Complexes

R	Ph	Ph	Ph	Ph	Ph	F	F	Ph	Ph
L	CO	NH_3	TCNE	Py	Py	Py	4-*t*-BuPy	void	$BuNH_2$
T	Py	Py	Py	$PMePh_2$	Py	Py	4-*t*-BuPy	oxo	oxo
FeN_4[a]	1.886	1.890	1.895	1.881	1.886	1.905	1.874	1.89	1.905
Fe-L[b]	1.789	2.03	1.850	2.055	1.999	2.055	2.027		2.070
Fe−T	2.067	2.04	2.018	2.298	2.051	2.048	2.030	1.709	1.760
				Displacements from N_4 Plane[c]					
δFe	0.079	0.05	0.047	0.042	0.092	0.055	0.056	−0.30	−0.026
δB	0.45	0.45	0.50	0.33	0.43	0.49	0.47	0.71	0.42
δC	0.14	0.09	0.08	0.11	0.27	0.13	0.14	0.09	0.06
δO	0.19	0.19	0.18	0.30	0.27	0.15	0.15	0.22	0.18
δMe	0.33	0.25	0.22	0.28	0.71	0.26	0.28	0.21	0.13
				Cavity Width and Axial Py Orientation					
at borons	6.37	6.37	6.42	6.46	6.47	6.37	6.24	6.17	6.42
at C_{para}	6.88	6.89	6.66	7.16	7.24	6.07(F)	5.93(F)	4.13	6.97
spread[d]	0.51	0.52	0.24	0.70	0.77			−2.04	0.55
ϕ_{Py} [e]	2.8	2.8	10. 2		7.2	2.0	9.4		
				78.8	79.8	81.5	83.3		86.3

[a] Average Fe−N_4 bond length. [b] Ligand bound inside cavity. [c] The maximum displacements of Fe, B, and dioxime C, O, and methyl carbon atoms are given. [d] Difference in cavity width at B and C_{para}. [e] Angle between Py (or Fe−N−Cα) plane and vertical plane through boron atoms.

Table 4. Structural Comparison of C_{2h} Structures[a]

	BPh_2 complexes					BF_2 complexes			
	11	**12**	**14**[1d]	**16**	**13**[1f]	**20**	**15**[1d]	**17**	**19**
L	CH_3CN	C_3H_7CN	$BuNH_2$	*i*-$PrNH_2$	MeIm	Cl	$BuNH_2$	*i*-$PrNH_2$	PIP
FeN_4	1.898(8)	1.886(5)	1.884(4)	1.89	1.89	1.898	1.877(6)	1.885	1.883
Fe−L	1.941	1.926(5)	2.053(4)	2.046	2.02	2.233(1)	2.047(4)	2.063	2.132
				Displacements from N_4 Plane[b]					
δ Fe	0.0	0.0	0.0	0.0	0.0	0.0	0.0	0.0	0.0
δ B	0.45	0.37	0.36	0.46	0.30	0.30	0.48	0.44	0.40
δ C	0.05	0.09	0.05	0.04	0.08	0.04	0.06	0.06	0.05
δ O	0.19	0.22	0.23	0.18	0.27	0.17	0.12	0.17	0.17
δ Me	0.17	0.32	0.24	0.23	0.33	0.16	0.22	0.20	0.20
θ tilt[c]	5.0	4.6	3.2	0.5	4.7	3.0	−1.8	0.5	0.7
pinch[d]	2.4	2.3	3.8	3.2	2.5	2.7	9.3	11.2	9.1
ϕ[e]			56	11	67		13	76	67[f]

[a] Distances in Å (typically ± 0.005 Å, angles in deg; details are given in the Supporting Information. [b] Displacement from N_4 plane. [c] Angle between Fe−L and a normal to the N_4 plane. [d] Angle between the axial B−R and Fe−L_{ax} vectors. [e] Dihedral angle between vertical plane through borons and the Fe−N−C_α plane. [f] Average of 64 and 71° for the two C_α's in PIP.

Structures Adopting the C_{2v} Conformation. (1)[1d] Fe((DMG)BPh_2)$_2$(Py)(CO)·CH_2Cl_2. The structure of this and the related BF_2 analogue, **2**, were reported previously. In both cases the CO is bound on the structured face with the trans pyridine lying over the boroximate chelate rings.

(2)[1d] Fe((DMG)BF_2)$_2$(Py)(CO)·CH_2Cl_2. Only minor structural differences are noted between the BPh_2 and BF_2 derivatives. The axial B−F groups are pinched more inward, and the iron and boron displacements from the N_4 plane are somewhat greater than in **1**.

(3) Fe((DMG)BPh_2)$_2$(Py)(NH_3)·CH_2Cl_2. The NH_3 complex is isostructural with the CO derivative with positional parameters, virtually identical to those of **1**. The axial Fe−N bond lengths are 2.034(5) for NH_3 and 1.994(8) for the trans Py. The structural coincidence of **1** and **3** underscores the "buried" nature of the bound CO and NH_3 ligands within the cyclophane-like cavity. The Fe, NH_3, CH_2Cl_2, and Py ligands lie on a 2-fold axis. During the refinement it was found that the crystal contained a 30% occupancy of CO in the binding site (an artifact arising from a contaminant in the Fe((DMG)BPh_2)$_2$(Py)$_2$ starting material). This leads to greater uncertainty in some of the structural parameters.

The ammonia ligand necessarily experiences close N−H−Ph contacts; however the symmetry imposed disorder of the ammine hydrogens prevents a detailed analysis of the N−H π interactions. These details are better defined in the amine derivatives discussed below.

(4) Fe((DMG)BPh_2)$_2$(Py)(TCNE)·2 CH_2Cl_2. The TCNE complex crystallizes in the noncentrosymmetric space group $P2_1$. The TCNE ligand is bound in a monohapto geometry[8] and is positioned in face-to-face contact with two axial phenyls. The sandwiched geometry found here is unique. In TCNE−cyclophane adducts, the TCNE lies on an external face of the cyclophane.[9a] In solution, 2:1 (DAD) charge transfer complexes between arenes and TCNE are disfavored owing to entropic factors.[10] In crystals of the 1:1 adduct of TCNE with hexamethylbenzene[9b] or cyclophanes,[9a] the TCNE is disordered between two symmetrical orientations over the phenyls. Thus **4** is the first structural characterization of a 2:1 TCNE−donor adduct and the only example in which TCNE adopts an ordered geometry.

The Fe−nitrile bond length of 1.85 Å is significantly shorter than the 1.94 Å length observed in bis(nitrile) complexes (**11**, **12**) but not strictly comparable to them. The latter adopt the C_{2h} conformation and lack the trans Py ligand of **4**. The iron atom (0.047 Å) and two borons (0.50 A) are displaced above

(8) For other binding modes of TCNE in metal complexes see: Kaim, W.; Moscherosch, M. *Coord. Chem. Rev.* **1994**, *129*, 157.
(9) (a) Saheki, M.; Yamada, H.; Yoshioka, H.; Nakatsu, K. *Acta Crystallogr.* **1976**, *B32*, 662. (b) Bernstein, J. Trueblood, K. N. *Acta Crystallogr.* **1971**, *B27*, 2078. (c) Becker, P.; Coppens, P. Ros, R. K. *J. Am. Chem. Soc.* **1973**, *95*, 7604. (d) Dixon, D. A.; Miller, J. S. *J. Am. Chem. Soc.* **1987**, *109*, 3656.
(10) Liptay, W.; Rehm, T.; Wehning, D.; Schanne, L;. Baumann, W. Lang, W. *Z. Naturforsch.* **1982**, *37A*, 1427.

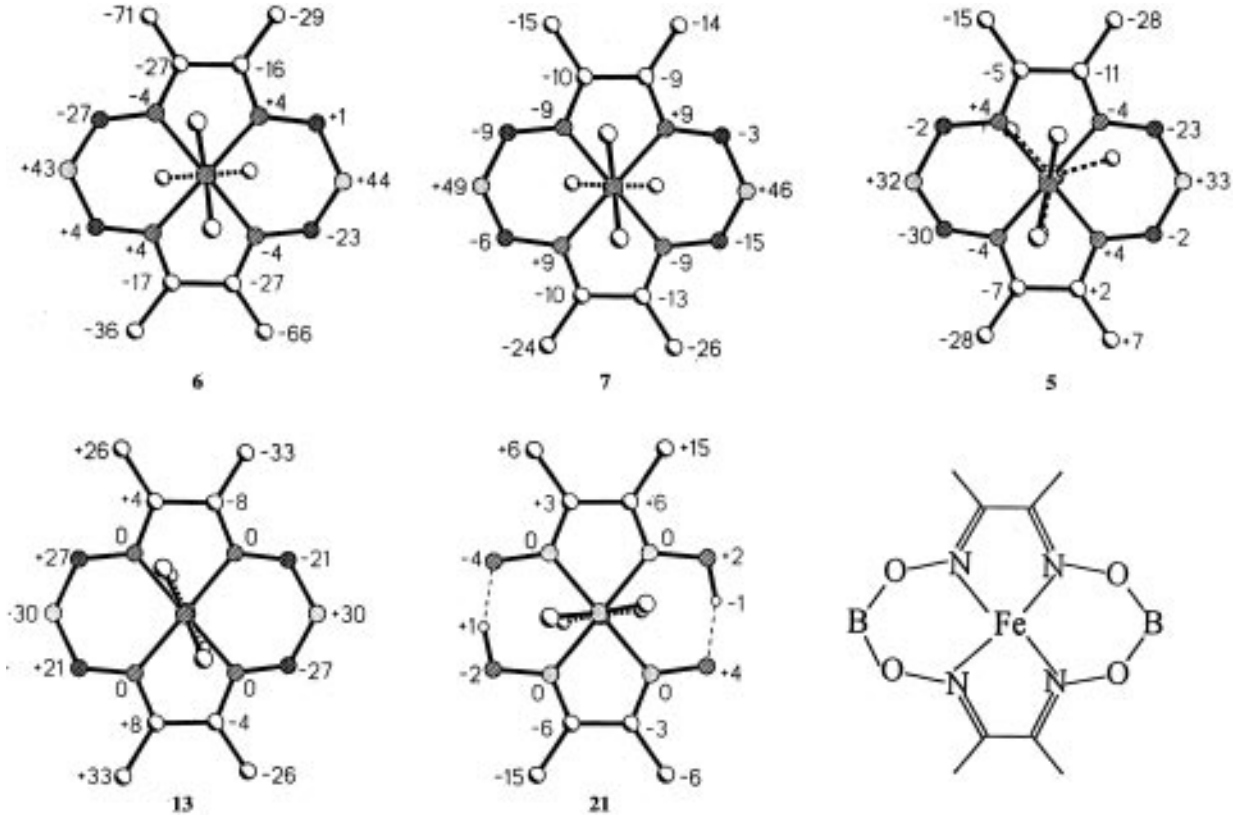

Figure 2. Diagrams showing the axial ligand orientation in selected complexes. The α-carbons of the axial ligand are shown projected onto the N_4 plane. Perpendicular displacements of ring atoms, in units of 0.01 Å, from the mean N_4 plane are given (+ is toward the cyclophane cavity in C_{2v} cases). Data for **13** and **21** are from refs 1f and 6a, respectively.

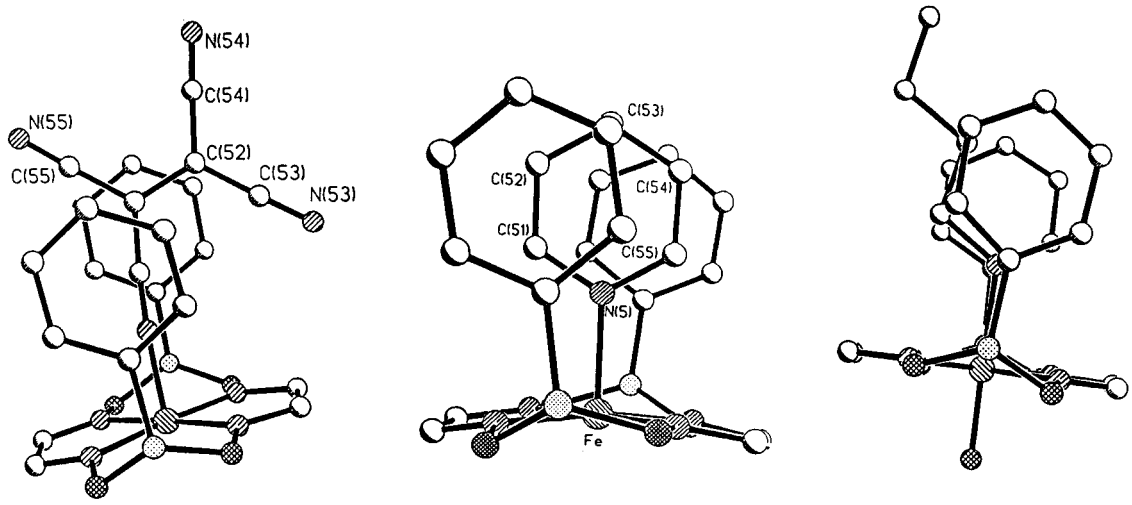

Figure 3. Partial structures showing the sandwiched TCNE ligand in **4**, Py in **6**, and $BuNH_2$ in **10** as viewed perpendicular to the axial ligand plane.

the N_4 plane toward the sandwiched TCNE ligand. The plane of the trans pyridine ligand makes an angle of 79° with the TCNE plane. The trans Fe−N_{py} bond is marginally shorter than those of the other complexes listed in Table 3.

In **4** the TCNE−phenyl contacts are largely predetermined by coordination to the iron macrocyclic complex. Only the lower half of the bound TCNE lies in contact with the phenyls (see Figure 3). The plane of the TCNE ligand lies 3.3 Å from the two parallel phenyl planes. This distance is similar to the interplanar separations in reported structures of other arene−TCNE adducts.[9] The metrical details of the TCNE ligand are unremarkable. Only minor structural effects typically accompany the formation of charge transfer complexes of TCNE.[8] The bond lengths in TCNE are not especially sensitive to "charge transfer" and even in cases where a full electron is transferred, as in $TCNE^-$ ion or M^+TCNE^- complexes, the central C−C bond is lengthened by <0.04 Å.[8,9e] The C−C bond in **4** of 1.388(10) Å shows some bond lengthening relative to TCNE[9d] (1.355(2)Å).

Other effects found in **4** are a 0.02 Å lengthening of the N(5)−C(50) bond and a 0.02 Å shortening of the C(50)−C(51) bond associated with the coordinated nitrile group. These differences are consistent with the effects of back-donation from the Fe. Effects of Fe−TCNE backdonation[1d] in **4** are evident in its redox potentials, in the low energy charge transfer band in the near−IR spectrum, and in the internal bond lengths in

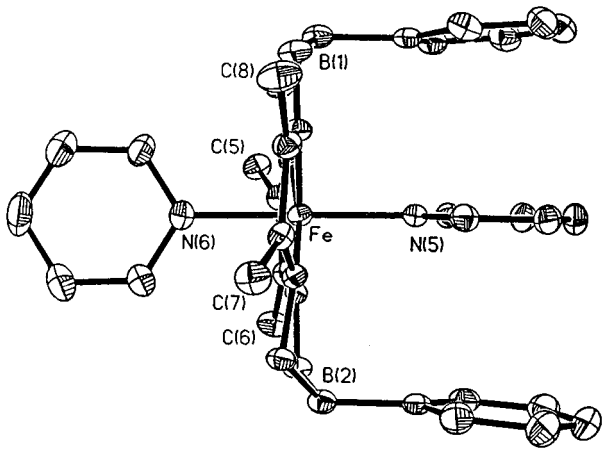

Figure 4. Side view of **6** showing the orientation of the Py ligands and the displacement of C(5) and C(7) below the N_4 ligand plane. Equatorial phenyl groups are omitted.

the TCNE ligand. Coulombic interactions between the TCNE and the phenyl groups are structurally invisible but they are largely responsible for a 4.6 kcal/mol stabilization of the bound TCNE over that in the BF_2 analogue.[1c] The Coulombic force depends primarily on the match of electrostatic surfaces of the interacting fragments and only slightly ($1/r$) on the distance between them.

(5) Fe((DMG)BPh_2)$_2$(Py)(P$MePh_2$). This complex crystallizes with no included solvent in the triclinic space group $P\bar{1}$. The bulky phosphine ligand is seen to enforce a C_{2v} conformation which sandwiches the pyridine ligand as predicted from ^{1}H NMR data.[1a] A similar sandwiched environment for pyridine is found in **6**. The Fe−P bond length is 2.298(2) Å. The Fe atom is displaced toward the Py ligand by 0.042 Å, which partially relieves the face strain associated with it. The axial phenyl and pyridine rings are parallel to each other but mutually twisted with respect to the symmetry axes of the FeN_4 unit by 12°.

(6) Fe((DMG)BPh_2)$_2$(Py)$_2$. Contrary to previous assumptions[1a−d] and in sharp contrast to the reported C_{2h} structure for the 1-MeIm analogue (**13**),[1f] **6** crystallizes in the C_{2v} conformation. This results in distinct environments for the two pyridine ligands, one sandwiched within the cyclophane-like cavity, the other lying on the open face of the iron complex. The iron atom lies 0.092 Å above the N_4 plane and the borons are also displaced to the same side by 0.44 Å. The sandwiched pyridine ligand (N(5)) is nearer to the iron than the pyridine on the open face (N(6)) but the latter is closer to the N_4 plane. A significant distortion of the N_4 ligand occurs indicative of face strain effects for the pyridine ligand. A displacement of two Fe−N═C bonds below the N_4 plane is amplified into a 0.7 Å displacement of a diagonal pair of methyl groups (C(5) and C(7)) below the N_4 plane. This distortion, shown in Figures 2 and 4, arises from face strain and is discussed in more detail below.

The sandwiched Py environment is found in both **5** and **6**. The plane of the sandwiched Py lies 3.6 Å from the phenyls in **5** and 3.4 Å in **6**. These distances are only slightly greater than the 3.3 Å separation of the TCNE and phenyl planes in **4**.

(7) Fe((DMG)BF_2)$_2$(Py)$_2$. A C_{2v} geometry is also observed for the bis(pyridine) complex in the BF_2 system. In this case the iron lies 0.055 Å above the N_4 plane, the Fe−N_{py} bond lengths are nearly equal. A distortion of the tetradentate N_4 ligand, characteristic of face strain, is also seen here but the distortions are about half as great as in **6**. The face strain effects are assumed to be similar in the two systems but the strain energy is distributed differently. With this assumption, the $\Delta\Delta G$ for the bis(pyridine) complexes reported previously remains a valid measure of axial repulsion except that the strain is concentrated in a single pyridine ligand and not divided equally between the two, as would be the case in a C_{2h} structure.

(8) Fe((DMG)BF_2)$_2$(4-*t*-Bupy)$_2$·2 CH_2Cl_2. This complex like **6** and **7** is found in the C_{2v} conformation. The structure mirrors effects described above for **7**. The *tert*-butyl groups are disordered in this complex and two CH_2Cl_2 solvent molecules flank the pyridine ligand on the open face. The fact that the C_{2v} structure is found in all three bis(pyridine) complexes is a strong indication that face strain effects associated with the pyridine ligands and not axial contacts or packing forces are responsible.

(9)[1e] [Fe((DMG)BPh_2)$_2$]$_2$O. The two μ-oxo structures, **9** and **10**, were reported previously. In both complexes the axial phenyls are constrained to the face trans to the oxo bridge. In the pentacoordinate species, **9**, the iron lies 0.3 Å out of the N_4 plane toward the oxo group with a bent Fe−O−Fe (166.0°). The collapse of the cyclophane-like cavity trans to the oxo group is a unique feature of this complex and is discussed in detail elsewhere.[1e] In the context of this work, **9** reveals the extent of cavity movement which is possible in the C_{2v} geometry and provides a model for the geometry of the pentacoordinate intermediate produced in dissociative substitution reactions of FeN_4 complexes.

(10)[1e] [($BuNH_2$)Fe((DMG)BPh_2)]$_2$$O_2$·2 $CHCl_3$. In the $BuNH_2$ ligated μ-oxo complex a linear (Fe−O−Fe 178.6°) bridge is observed with the iron atoms only slightly displaced (0.026 Å) from the N_4 planes. The $BuNH_2$ ligand is sandwiched within the cyclophane-like cavity. The cavity has opened up to a size similar to that found in monomeric Fe(II) derivatives which adopt the C_{2v} geometry. The presence of two axial phenyls surrounding the bound $BuNH_2$ ligand constrains the axial ligands to lie over the diimine rings of the FeN_4 complex ($\phi = 86.3°$. This feature has significant implications for facially hindered ligands such as Py and *i*-$PrNH_2$, and it is believed to enhance the allosteric effects found in the μ-oxo derivatives.[1g,h]

Structures Adopting the C_{2h} Conformation. (11) Fe((DMG)BPh_2)$_2$(CH_3CN)$_2$·2 CH_3CN and (12) Fe((DMG)BPh_2)$_2$($CH_3CH_2CH_2CN$)$_2$. The two nitrile complexes both have similar centrosymmetric C_{2h} structures with the iron atom constrained by symmetry to lie in the N_4 plane. The CH_3CN derivative crystallizes with two CH_3CN solvent molecules. In the butyronitrile derivative, the γ-carbon of the butyronitrile ligand is disordered between two positions. In one conformation (sof = 0.6) a single α-C−H is directed toward the center of the axial phenyl while in the other (sof = 0.4) two α-hydrogens are directed to the edge of the phenyl ring. The site occupancies may reflect subtle energetics associated with the axial Ph contacts.

(13) Fe((DMG)BPh_2)$_2$(1-MeIm)$_2$·2 CH_2Cl_2. Crystals of this complex were independently examined and found to have a C_{2h} structure identical to that previously reported by Jansen and Verhage.[1f] The two axial 1-MeIm ligands lie over the diimine rings in the same plane with $\phi = 67°$. In $Fe(DMGH)_2(Im)_2$, the imidazole ligands are also coplanar but lie over the dioximate rings at $\phi = 7°$.[6a] The C_{2h} structure for the 1-MeIm derivative stands in sharp contrast to results for the Py derivatives above underscoring the significant effect which can arise from the subtle steric differences between imidazole and pyridine ligands.

(14)[1d] Fe((DMG)BPh_2)$_2$($BuNH_2$)$_2$. This and the related BF_2 complex, **15**, are both found in the C_{2h} conformation. In **14** the $BuNH_2$ faces a single phenyl with one N−H bond directed toward the center of the phenyl ring with the α-C directed over an Fe−N bond at $\phi = 56°$. In the sandwiched $BuNH_2$ found

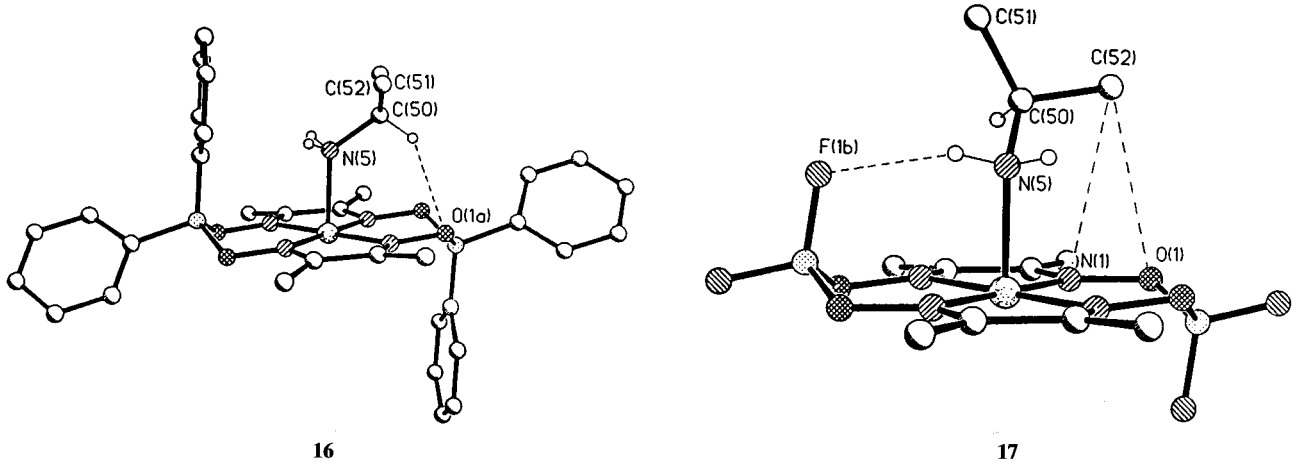

16 **17**

Figure 5. Orientation of bound *i*-$PrNH_2$ in **16** and **17**. The N−H−F hydrogen bond in **17** and some repulsive contacts are shown. The centrosymmetrically disposed trans ligand is omitted.

in the μ-oxo derivative, **10**, the N−H bonds are each pointed toward a phenyl ring with the N−C vector directed between the two axial phenyl groups at $\phi = 86.3°$. Weakly attractive N−H π interactions are considered insignificant compared to other repulsive interactions in determining the orientation of the bound $BuNH_2$ ligand.

(15)[1d] Fe((DMG)BF_2)$_2$($BuNH_2$)$_2$. A C_{2h} structure similar to **14** is observed. A hydrogen bond between the $BuNH_2$ and an axial fluorine constrains the N−C_α bond to lie over the opposite boroximate ring ($\phi = 13^o$). The N−Fe−N axis is tilted slightly toward the axial fluorines here while it is tilted away from the axial phenyls in **14**. Thermodynamic data do not indicate significant differences in the $BuNH_2$ binding to the BF_2 and BPh_2 systems as a result of these interactions.[1c]

(16) Fe((DMG)BPh_2)$_2$(*i*-$PrNH_2$)$_2$·2 CH_2Cl_2. A C_{2h} conformer is observed with an axial Fe−N distance of 2.05 Å similar to that in **14**. The major difference between the $BuNH_2$ and *i*-$PrNH_2$ complexes lies in the orientation of the amine with respect to the angle ϕ and the presence of an unusual **eclipsed conformation** about the amine N−C_α bond. The eclipsing about the N−C bond is a necessary condition for maximizing the methyl−N_4 plane distances. In a staggered conformation β-methyl−N_4 plane contacts would be prohibitive (2.3 Å) and even in the eclipsed conformer the β-methyl carbons lie only 3.7 Å from the N_4 plane. The α-CH bond is directed toward the N_4 plane but finds a space 2.33 Å above the boroximate ring. While contacts as close as 2.5 Å are produced, Coulombic factors may reduce the repulsive nature of these contacts. The torsional strain associated with the enforced eclipse within the *i*-$PrNH_2$ ligand may account for most of the reduced binding affinity of *i*-$PrNH_2$ compared with $BuNH_2$.

(17) Fe((DMG)BF_2)$_2$(*i*-$PrNH_2$)$_2$. This complex was refined in $P\bar{1}$ with $Z = 2$. Two independent half-molecules make up the asymmetric unit with each iron lying on a center. One N−H forms an intramolecular hydrogen bond with an axial fluorine. The other forms an intermolecular hydrogen bond with an axial fluorine of a neighboring molecule. This makes each amine nitrogen chiral. One half-molecule consists of a single chirality which along with its antipode produces an ordered meso full molecule. Both orientations (chiralities) are found in the other half molecule and a disordered full molecule results. The disorder arises depending on which of the two diastereotopic N−H hydrogens are used for the distinct hydrogen bonds. A pattern of alternating ordered and disordered full molecules results.

The Fe−N_{ax} bond length is almost the same as for **16**. The N−C_α bond dihedral angle is 28^o lying halfway between the staggered and eclipsed geometries. The intramolecular N−H−F hydrogen bond constrains the N−C_α bond to project over the diimine ring. Rotation about this bond (starting at the eclipsed geometry of **16**) moves one isopropyl methyl toward the N_4 plane giving contacts of 3.35 Å with N(1) and O(1) while the α-CH moves away from the N_4 plane with its closest contacts now at 2.9 Å. The orientation enforced by the hydrogen bond places the methyl more comfortably over the boroximate ring while leaving the α-CH projecting over the diimine ring but now 2.9 Å from it. The result is a reasonable compromise between the hydrogen bonding, face strain, and torsional strains involved.

(18) Fe((DMG)BPh_2)$_2$(PIP)$_2$·2 CH_2Cl_2. Only a crystallographically marginal crystal[11] could be obtained, which lost solvent during data collection. An isotropic refinement adequately establishes the gross features which resemble closely those of **19** below. These include a C_{2h} conformer and Fe−N_{ax} bond lengths of 2.15(1) Å. The PIP orientation differs only slightly from that in **19**. The single N−H on each PIP ligand is directed toward the center of the axial phenyl ring and lies 2.4 Å from it. A smaller tilt angle (0.5°) and a reduced displacement of the borons from the N_4 plane (0.3 Å) compared to **14** appear to be a consequence of the opposing repulsive factors of axial and facial strain. An increase in the tilt would aggravate the facial α-CH contacts.

(19) Fe((DMG)BF_2)$_2$(PIP)$_2$. A C_{2h} conformer is found. The Fe−N_{pip} bond length is 2.132(2) Å comparable to that for **18** and also to the 2.127 Å bond length reported for Fe(TPP)-(PIP)$_2$.[5b] The PIP orientation in terms of the angle ϕ is largely determined by the N−H−F hydrogen bond. The PIP ligand has 4 α-CH bonds directed toward the N_4 plane giving rise to a more significant but better distribution of strain across the N_4 ligand face than in $BuNH_2$ or *i*-$PrNH_2$. Several facial contacts in the 2.6−2.7 Å range are found but no significant distortions, other than the Fe−N_{ax} bond lengthening, are evident.

(20) [Et_4N][Fe((DMG)BF_2)$_2$(Cl_2)]. This is the only structurally characterized monomeric Fe(III) derivative in these systems and only the second example of a low spin Fe(III) complex containing the weak field chloride ligand. The tetraethylammonium cation lies on a center and displays a common form of disorder. The centrosymmetric anionic iron complex also lies on a center of symmetry. The Fe(III)−N bond lengths (1.89

(11) Crystal data: space group $P\bar{1}$, $a = 10.318(6)$Å, $b = 10.674(12)$Å, $c = 11.570(11)$Å, $\alpha = 88.7(1)°$, $\beta = 70.31(6)°$, $\gamma = 89.66(9)°$. 2230 data/103 parameters. R ($I > 4\sigma$) = 0.12 (isotropic). Details are given in the Supporting Information.

Å) are indicative of a low spin state confirmed by EPR measurements[12] and are not significantly different from the Fe−N bond lengths in the Fe(II) or μ-oxo-Fe(III) derivatives above. The Fe−Cl bonds lie parallel to and eclipse the B−F bonds with F−Cl contacts at 2.30 Å. The Fe−Cl bond length (2.233(1) Å) is slightly shorter than that reported for the cationic low spin Fe(III) complex of a saturated tetradentate macrocycle, *trans*-$[Fe(diac H_2)Cl_2]^+$ (2.248(1)[13]). The Fe−Cl bond lengths in pentacoordinate high spin hemin chlorides (2.218(6) Å, Fe(protoIX)(Cl);[14] 2.193(3) Å, FeTPPCl[15]) are somewhat shorter. Axial bond shortening is favored by the low spin state, lower coordination number, and displacement of the Fe from the N_4 plane. In hemin chlorides the latter two factors offset the bond length expansion normally associated with the high spin state.

Discussion

Some differences between these systems and the well established stereochemical characteristics of hemes[7] are worth noting. The FeN_4 distances of 1.89 Å are 0.1 Å shorter than those typical of low spin hemes. This reflects the smaller hole size of 14 vs 16 membered macrocyclic rings.[16] The FeN_4 systems lack the D_{4h} symmetry of hemes and have at most 2-fold rotational symmetry. In the larger porphyrin ring, the pyrrole α-carbons are 3.0 Å from a low spin Fe atom in contrast to a typical 2.7 Å distance for the imine carbons or oxime oxygen atoms in $Fe((DMG)BR_2)_2$ complexes. As a result, face strain effects are much more important in the smaller macrocycles.

The six-membered (boroximato)iron rings are puckered, in contrast to the usual planarity of hemes, leading to the C_{2v} and C_{2h} conformations observed for the FeN_4 complexes. Axially directed substituents on boron generally lie closer to iron bound ligands than peripheral substituents such as the phenyl caps of capped porphyrins,[3a,b] the pivalamide pickets of picket fence[3c] porphyrins, or the isophthalamido walls of picnic basket[3d,e] porphyrins. Cross cavity dimensions in the C_{2v} conformer of the FeN_4 systems are shorter and ligand-cavity wall contacts significantly closer than those found in the picnic basket porphyrin structures Ru(C6-PBP)(Py)(CO)[3c] and Ru(C6-PBP)-$(Py)_2$.[3d] The sandwiched pyridine in **6** has wall contacts in the 3.3−3.5 Å range while no wall contacts with Py in Ru(C6-PBP)$(Py)_2$ are less than 3.8 Å. Even in the simple carbonyl complex, **2**, the axial fluorines are in closer contact[1d] with the bound CO than are atoms of the phenyl cap of the more elaborate $Fe(C_2$-Cap)(1-MeIm)(CO) complex.[3b]

The borylated dioxime complexes, in comparison with many superstructured hemes, show much smaller and less complex structural distortions of the macrocycle and its superstructure. At the same time they achieve more intimate nonbonded contacts between the ligand and the superstructure. This gives us confidence in the assignment of ligational differences between BF_2 and BPh_2 systems to specific nonbonded interactions and provides a firmer basis upon which to evaluate other effects.

Metrical Details of the C_{2v} and C_{2h} Conformers. Some important structural parameters are compared in Table 3 (C_{2v}) and Table 4 (C_{2h}). The FeN_4 unit shows negligible differences in the Fe−N_4 bond lengths with an average value of 1.89 A. The geometry and bond lengths within the N_4 macrocycle are similar in all derivatives. A displacement of the boron atoms above the N_4 plane of about 0.42 Å is typical. Somewhat smaller displacements occur when both ligands are bulky as in **5** while much greater values accompany the cavity collapse around the void in the μ-oxo complex, **9**.

In the centrosymmetric C_{2h} cases the metal atom is constrained to lie in the N_4 plane. In the C_{2v} conformer, the position of the Fe atom with respect to the N_4 plane is determined by the nature of two axial ligands. The Fe lies from 0.04 to 0.092 Å above the N_4 plane on the same side as the two boron atoms. In **5** the $PMePh_2$ lies on the open face consistent with the notion that $PMePh_2$ is more bulky with respect to axial interactions than Py. The iron atom however is displaced toward the Py ligand, suggesting that the Py experiences the greater face strain. In the μ-oxo species, **9** and **10**, the iron is displaced toward the oxo ligand and away from the borons. These are the only cases where the Fe atom and axial superstructure lie on opposite faces.

The cyclophane-like binding cavity expands or contracts in response to axial interactions. A spread coordinate defined as the difference between the B−B and C−C_{para} separations gives a measure of the spreading of the cavity as one moves out from the iron atom. In the pentacoordinate μ-oxo species the cavity folds inward to fill the void giving a negative spread. Of the remaining cases, the TCNE shows the smallest spread and the smaller CO, NH_3, and $BuNH_2$ ligands produce intermediate spreads of 0.5 Å while the two examples with Py sandwiched inside the cavity **5** and **6**, show the greatest spreads. The spread values correlate with measures of phenyl-substrate interactions derived from our previous ligand binding studies.[1c] Values of $\Delta\Delta G$ are −4.6, −0.3, and +2.7 kcal/mol for TCNE, CO, and Py respectively. The dramatic differences for TCNE and Py reflect the importance of Coulombic factors in face-to-face $\pi-\pi$ interactions.[1c,17]

Conformational Preferences. The preferred conformation in $Fe((DMG)BR_2)_2$ complexes (both in the solid state and in solution[1c]) is primarily determined by the 1,4-diaxial contacts in the boroximato−iron rings. The C_{2h} conformer is found in the symmetrically ligated species, **11**−**20**, while the C_{2v} conformer is favored when the two axial ligands differ.

The bis(pyridine) complexes, (**6**, **7**, **8**) are the only examples where the C_{2v} conformation is found for a symmetrically ligated complex. In the C_{2v} conformer, the two pyridine ligands lie in mutually perpendicular planes, thus permitting face-strain relief via the distortions shown in Figure 2 and Figure 4. In a C_{2h} conformer both pyridines would lie in approximately the same plane as in **13** (see Figure 1) producing opposing facial pressures on the five membered Fe−diimine rings. Severe lengthening of the Fe−N_{ax} bond as witnessed in the PIP derivative, **18**, would be required to relieve Py face-strain in a C_{2h} structure.

Face Strain. Face strain effects are well established for the 2-MeIm ligand[7] and have been invoked to explain the longer Fe−N bond lengths of piperidine and pyridine vs imidazole ligands in hemes.[5b,7] The ortho hydrogens of an axial pyridine lie about 0.3 Å closer to the N_4 plane than those of an identically bound imidazole ligand leading to significantly greater facial strain.

A reasonable distinction between the effects of axial and face strain can be made by comparing ligand binding data for the BF_2 and BPh_2 systems. Table 5 summarizes experimental data for the free energies of formation of complexes (eq 1) and the rate constants for ligand dissociation (eq 2).

Large differences in ΔG^o (eq 1) between BF_2 and BPh_2 systems primarily reflect axial strain associated with phenyl - ligand interactions. The differences in ΔG^o for L = $BuNH_2$, *i*-$PrNH_2$, and PIP are small and were assigned previously[1c] to

(12) Stynes, D. V.; Noglik, H.; Thompson, D. W. *Inorg. Chem.* **1991**, *30*, 4567.
(13) Curtis, N.; Xin, L.; Weatherburn, D. C. *Inorg. Chem.* **1993**, *32*, 5838.
(14) Koenig, D. F. *Acta Crystallogr.* **1965**, *18*, 663.
(15) Hoard, J. L.; Cohen, G. H.; Glick, M. D. *J. Am. Chem. Soc.* **1967**, *89*, 1992.
(16) Hung, Y.; Martin, L.; Jackels, S. C.; Tait, M.; Busch, D. H. *J. Am. Chem. Soc.* **1977**, *99*, 4029.
(17) Hunter, C. A.; Sanders, J. K. M. *J. Am. Chem. Soc.* **1990**, *112*, 5525.

Table 5. Energetic and Structural Factors[a] in Ligand Binding to $Fe((DMG)BR_2)_2$

$L_{ax} = L'$	R	ΔG^{o} [b]	k_{-L}, s^{-1} [c]	ΔG_{face} [d]	$Fe-L_{ax}$, Å	α-H contact,[e] Å
$BuNH_2$	Ph	14.05	0.013	0.0, 0.0	2.053(4)	2.62 (O)
	F	14.45	0.013	0.0, 0.0	2.047(4)	2.65 (O)
1-MeIm	Ph	>14	0.008[f]	- - -, −0.30	2.02(1)	2.61 (N)
	F	>14	0.0013[f]	- - -, −1.30		
i-$PrNH_2$	Ph	9.65	1[g]	4.6, 2.6	2.046(7)	2.44 (O)
	F	10.25	1[g]	4.2, 2.6	2.063(2)	2.92 (C)
PIP	Ph	8.23	76[f]	5.8, 5.1	2.153(12)	2.49 (C)
	F	8.85	16[f]	5.6, 4.2	2.132(2)	2.58 (C)
Py	Ph	6.38	6.5	8.1, 3.7	2.051(3)	2.47 (O)
					1.999(3)[h]	2.59 (C)
	F	9.0	0.15	5.5, 1.4	2.048(6)	2.52 (O)
					2.055(5)[h]	2.55 (C)
2-MeIm	Ph	1.95		12.1, - - -		
	F	5.73	160[i]	8.7, 5.6		
L_{ax}	$(L' = Py)$[j]					
TCNE	Ph	12.5	0.0006		1.850	
	F	7.9	20			
$MePZ^+$	Ph	9.57	0.15			
	F	7.70				

[a] Kcal/mol at 298 K, CH_2Cl_2 solution. [b] Free energy of formation from $Fe((DMG)BR_2)_2(CH_3CN)_2$ from ref 1c. [c] Dissociation rate of L (eq 2) from ref 1d. [d] Free energy difference relative to $BuNH_2$: the first entry is based on $\Delta G°$, the second on $RT \ln(k_{-L}/k_{-Bu})$. [e] The closest contact is given. [f] Toluene solution, ref 1d. [g] Estimated from data in ref 1c. [h] Pyridine bound on structured face. [i] Stynes, D. V.; de Silva, D. G. A. H.; Thompson, D. W. *Inorg. Chim. Acta* **1991**, *188*, 139. [j] Data trans to Py from ref 1c; $MePz^+$ is the *N*-methylpyrazinium ion.

$$FeN_4(CH_3CN)_2 + 2L \rightleftarrows FeN_4L_2 + 2CH_3CN \qquad (1)$$

$$FeN_4L_2 \rightarrow FeN_4L + L \qquad (2)$$

a slightly greater Lewis acidity of the BF_2 system as a result of inductive effects. Only Py and 2-MeIm are seen to suffer significant axial strain as shown by the large difference in ΔG^o between the BF_2 and BPh_2 systems. Ligands presenting regions of positive surface charge density such as TCNE, methylpyrazinium ion ($MePz^+$), and others[1c] experience a net attractive interaction with the axial phenyls.

There is good reason to believe[18] that face strain is the dominant factor in the different amine binding affinities shown in Table 5. In pentacoordinate Co(porphyrin)(L),[19] ZnTPP(L),[20] $Fe(C_n\text{-CAP})L$[3a] or high spin hemes,[21] the longer metal−ligand bond lengths and large displacements of the metal from the N_4 plane combine to significantly reduce face strain effects. In these cases Py, PIP, and 1-MeIm have similar binding strengths and 1,2-Me_2Im binds more strongly than 1-MeIm.[21] However, in six-coordinate low spin heme, FePc, or FeN_4 systems, 1-MeIm is a much better ligand compared to Py or PIP, and 1,2-Me_2Im is prohibitively weak.[22] A connection between face strain and the ortho effect described by Traylor[2a] may account for the significantly improved binding of pyridine to certain atropisomers of ZnTPivP[20b] and other anomalies found in some strained tetraphenylporphyrin based systems.

In an attempt to quantify the face strain, we have used the relatively unhindered $BuNH_2$ ligand as a reference zero and calculated thermodynamic and kinetic differences within each $Fe((DMG)BR_2)_2$ system for the various amines. The results are listed as ΔG_{face} in Table 5, although effects other than facial strain are certainly involved. The ΔG_{face} values suggest a facial hindrance order for the amines: PIP > *i*-$PrNH_2$ > $BuNH_2$ and 2-MeIm > Py > MeIm. This order is consistent with the α-CH contacts found in the structural data above. For Py and *i*-$PrNH_2$ the kinetically derived parameter is much lower than that based upon $\Delta G°$. In these cases, orientations favorable to the relief of face strain in the trans ligand are possible in a C_{2v} transition state.

Axial Ligand Orientation. The orientation of imidazole and pyridine ligands with respect to the N_4 plane in hemes[23−25] and other macrocycles[26] has been the subject of considerable interest. Both electronic and steric factors have been considered. A dominant role for nonbonded interactions between ortho (α) hydrogens and the N_4 plane are indicated from our results. In the five examples of axially enforced pyridine or imidazole orientation (**5**, **6**, **7**, **8**, and **13**) the axial ligand plane does not bisect the diimine chelate ring but rather points toward the carbon of one of the two C═N bonds therein (see Figure 2).

The orientation of the $N-C_\alpha$ bond of the $BuNH_2$ and *i*-$PrNH_2$ ligands in **14** and **16** appears to be controlled by a combination of axial and and α-CH facial contacts. The $BuNH_2$ ligand is found in the stable staggered conformation with two α-CH bonds projected toward the N_4 plane where they flank one of the Fe−N bonds. The eclipsed *i*-$PrNH_2$ gives a single α-CH -N_4 interaction with the hydrogen projected into the space above

(18) log K_1 for binding to CoPPIXdme[19] in toluene 23 °C: 3.78 (Py), 3.70 (1-MeIm), 3.83 (PIP). log K_1 for binding to Zn(T-*p*-CH_3PP):[20a] 4.40 ($BuNH_2$), 4.84 (PIP), 3.52 (Py), 4.66 (1-MeIm). log K_1 for binding to Zn(α^4-TpivPP) in toluene, 25 °C: 4.38 (Py), 5.60 (PIP). log K_1 for binding to Zn(*trans*-α^2-TpivPP): 5.70 (Py), 5.46 (PIP).[20b] log K_1 for binding to Fe(DHD)[21] in benzene, 25 °C: 3.65 (Im), 3.67 (4-CNPy), 4.11 (2-MeIm) log K_1 for binding to open face of capped hemes[3a] in toluene, 23 °C: $Fe(C_2\text{-CAP})$, 2.90 (1-MeIm), 3.06 (1,2-Me_2Im, 2.25 (*n*-$PrNH_2$) 2.15 (*sec*-$BuNH_2$); Fe(C3-CAP), 3.32 (1-MeIm), 3.61 (1,2-Me_2Im), 3.40 (*n*-$PrNH_2$), 2.79 (*sec*-$BuNH_2$).

(19) Stynes, D. V.; Stynes, H. C.; James, B. R.; Ibers, J. A. *J. Am. Chem. Soc.* **1973**, *95*, 1796.

(20) (a) Imai, H.; Nakagawa, S.; Kyuno, E. *J. Am. Chem. Soc.* **1992**, *114*, 6719. (b) Imai, H.; Kyuno, E. *Inorg. Chem.* **1990**, *29*, 2416.

(21) Brault, M.; Rougee, D. *Biochemistry* **1975**, *14*, 4100.

(22) (a) Stynes, D. V.; James, B. R. *J. Am. Chem. Soc.* **1974**, *96*, 2733. (b) Weschler, C. J; Anderson, D.; Basolo, F. *J. Am. Chem. Soc.* **1974**, *97*, 6707. (c) Lavellette, D.; Tetreau, C.; Momenteau, M. *J. Am. Chem. Soc.* **1979**, *101*, 5395.

(23) (a) Scheidt, W. R.; Chipman, D. M. *J. Am. Chem. Soc.* **1986**, *108*, 1163. (b) Rohmer, M.; Strich, A.; Veillard, A. *Theor. Chim. Acta* **1984**, *65*, 219. (c) Hatano, K.; Safo, M.; Walker, F. A.; Scheidt, W. R. *Inorg. Chem.* **1991**, *30*, 1643.

(24) Geiger, D. K.; Lee, Y. J.; Scheidt, W. R. *J. Am. Chem. Soc.* **1984**, *106*, 6339.

(25) (a) Scheidt, W. R.; Geiger, D. K.; Haller, K. J. *J. Am. Chem. Soc.* **1982**. *104*, 495. (b) Scheidt, W. R.; Hayes, R. G.; Lang, G. *J. Am. Chem. Soc.* **1983**, 105, 2625. (c) Scheidt, W. R.; Geiger, D. K.; Lee,Y. J.; Reed, C. A.; Lang, G. *Inorg. Chem.* **1987**, *26*, 1039. (d) Safo, M.; Gupta, G. P.; Walker, F. A.; Scheidt, W. R. *J. Am. Chem. Soc.* **1991**, *113*, 5497. (e) Safo, M.; Gupta, G. P.; Watson, C. T.; Simonis, U.; Walker, F. A.; Scheidt, W. R. *J. Am. Chem. Soc.* **1992**, *114*, 7066.

(26) Gerli, A.; Sabat, M.; Marzilli, L. G. *J. Am. Chem. Soc.* **1992**, *114*, 6711.

the larger boroximate rings. In the BF_2 system (**15**, **17**, and **19**) an N−H−F hydrogen bond appears to control the axial ligand orientation.

London Forces. London dispersion forces are the weakest of the attractive interatomic forces. They should not be confused with more significant hydrophobic forces, which derive their energy from the strong interactions of water with itself, or with steric effects, which involve Pauli and Coulombic repulsions between electrons and between the atomic nuclei. In molecular mechanics calculations, a two-term or Lennard−Jones function[27a] is typically used to approximate van der Waals interactions.

$$E(\mathrm{VDW}) = \epsilon[(r^*/r)^{12} - 2(r^*/r)^6)] \qquad (3)$$

This equation includes both a repulsive steric effect ($1/r^{12}$) and the attractive London ($1/r^6$) forces, but omits the often more important Coulombic forces.[27b]

For reactions in solution, London forces are not easily dissected from stronger steric, solvation, conformational, Coulombic, and other effects. Nevertheless, London forces have been invoked to rationalize subtle effects within more elaborate binding cavities, where steric, electrostatic, and other effects are not adequately understood and where no structural data are available.[20a,28]

Structural data in $Fe((DMG)BPh_2)_2$ complexes show that most ligand atoms typically lie within the net attractive region of van der Waals interactions (eq 3). Some 40 Py−phenyl pairwise C−C contacts between 3.3 and 4.0 Å are present in **5** and **6**. However, both the ligation energetics (Table 5) as well as the increased spread coordinate (Table 3) suggest a net repulsive Py−Ph interaction. Any stabilization derived from intramolecular London attractions in **6** is likely duplicated by extramolecular solvational contacts with the axial ligands in **7** and/or offset by minor conformational strains associated with the slightly greater opening of the cavity.

The orientations of the bound ligands and subtle changes in the size and shape of the cavity are first adapted to minimize steric repulsions. This inevitably leaves atoms at or near van der Waals contact. There is no compelling evidence that these systems, or more complex ones[3,20b] take advantage of weak London forces to favor one ligand over another.

The design of cavities for selective binding is most effectively engineered on the basis of repulsive interactions (size and shape) or attractive Coulombic forces.[3] These forces, unlike London forces, cannot be duplicated by extramolecular solvation, but must be imposed by the primary structure.

Structure and Reactivity. In proteins, reactivity inferences based on structural data alone can be grossly in error if the molecular dynamics of the protein are ignored.[29,30] In simple molecules, bond length reactivity relationships are commonly assumed to exist, but real data showing such correlations are rare.[31] We have found that metal−ligand bond lengths can be unreliable[1d] as an indicator of binding energetics. Metal−ligand bond lengths fail to reflect the sometimes significant redistribution of energy which often accompanies ligand binding to a metal complex. The different $Fe-N_{py}$ bond lengths in **6** and the trends found for $BuNH_2$, *i*-$PrNH_2$, and PIP illuminate this point.

The sandwiched pyridine in **6** experiences repulsive contacts with the axial phenyls (evidenced by the slight opening of the cyclophane cavity) as well as significant face strain (evidenced by the distortion of the N_4 ligand) yet it has the shorter $Fe-N_{py}$ bond length. This dilemma stems from an inherent limitation of the localized bond concept. On thermodynamic grounds, only the sum of the two $Fe-N_{py}$ bond energies is observable. The position of the iron atom and the two $Fe-N_{py}$ bond lengths reflect a compromise between several competing factors: face and axial strain, FeN_4 and axial Fe−N bonding, etc.

The relative lability of the Py ligands provides the only basis for assigning individual bond strengths to them. In a more rigid picnic basket porphyrin system,[3e] $Ru(C6\text{-}PBP)(Py)_2$, it was established that the inside bound pyridine with a longer $Ru-N_{py}$ bond was more inert than the outside bound pyridine with a shorter bond! In our system we suggest, on intuitive grounds only, that the inside bound pyridine (with the shorter $Fe-N_{py}$ bond) is more labile. Experimental proof cannot be obtained here since conformational flipping, which interchanges the two environments, is more rapid than Py exchange.

For *i*-$PrNH_2$, the $Fe-N_{ax}$ bonds are only marginally shorter (**16** vs **14**) or longer (**17** vs **15**) compared to the $BuNH_2$ analogue in the two systems, but the binding of *i*-$PrNH_2$ is weaker in both. The face strain of *i*-$PrNH_2$ is accommodated largely by the introduction of torsional strain in the ligand. For PIP, $Fe-N_{ax}$ bond lengthening provides the face strain relief. One estimates about 3 kcal/mol in strain for eclipsing the *i*-$PrNH_2$ bond[32] or for stretching[33] the two $Fe-N_{pip}$ bonds by 0.1 Å. These factors are thus a major component of the ΔG_{face} differences between $BuNH_2$, *i*-$PrNH_2$, and PIP shown in Table 5.

The energetics of nonbonded interactions are critically dependent upon conformational constraints imposed by the particular system. The imposition or release of such constraints can provide an important control mechanism for their use. Even the relatively simple molecules described here possess a variety of options in resolving repulsive nonbonded conflicts. The effects on binding depend only on the least unfavorable option which as seen for *i*-$PrNH_2$, PIP, and Py can be completely different. In designing systems to make use of repulsive nonbonded interactions, one must effectively block all strain relief options. In contrast, attractive nonbonded contacts are their own reward and will spontaneously self-optimize within the conformational limits imposed by the system.

Face Strain Effects in μ-Oxo Complexes. The above results demonstrate how a few nonbonded interactions can exert significant control over the orientation and binding affinity of ligands. Allostery[34] which involves linked binding sites in complex multisubunit proteins poses a much greater biomimetic challenge.[35] In its simplest form cooperativity (positive or negative) is displayed when multiple identical sites communicate so that reaction at one site makes the same reaction at a second

(27) (a) Atkins, P. W. *Physical Chemistry*; W. H. Freeman and Co.: San Francisco, 1978; Chapter 23. (b) Nonbonded parameters: r^*(Å), ϵ-(kcal/mol): sp^3 C, 1.9080, 0.1094; sp^2 C, 1.9080, 0.0860; sp^2 N, 1.8240, 0.170; sp^2 O, 1.661, 0.210; H (arom), 1.459, 0.0157; hydrocarbon H, 1.487, 0.0157. Cornell, W. D.; Cieplak, P.; Bayly, C.; Kollman, P. A. *J. Am. Chem. Soc.* **1993**, *115*, 9620.

(28) (a) Diederich, F.; Dick, K.; Griebel, D. *J. Am. Chem. Soc.* **1986**, *108*, 2273. (b) Kobayashi, K.; Asakawa, Y.; Toi, H.; Aoyama, Y. *J. Am. Chem. Soc.* **1993**, *115*, 2648.

(29) Case, D. A.; Karplus, M. *J. Mol. Biol.* **1979**, *132*, 343.

(30) (a) Ray, G. B.; Li, X.; Ibers, J. A.; Sessler, J. L.; Spiro, T. G. *J. Am. Chem. Soc.* **1994**, *116*, 162. (b) Lim, M.; Jackson, T. A.; Anfinrud, P. A. *Science* **1995**, *269*, 962.

(31) Jones, P. G.; Kirby, A. J. *J. Am. Chem. Soc.* **1984**, *106*, 6207.

(32) Allinger, N. L.; Hirsch, J. A.; Miller, M. A.; Tyminski, I. J.; VanCatledge, F. A. *J. Am. Chem. Soc.* **1968**, *90*, 1199.

(33) The estimate assumes a harmonic potential with an N−Fe−N symmetric stretch force constant[2c] of 2.5×10^5 dyn/cm.

(34) Wyman, J., Jr. *Adv. Protein Chem.* **1964**, *19*, 223.

(35) (a) Traylor, T. G.; Mitchell, M. J.; Ciccone, J. P. Nelson, S. *J. Am. Chem. Soc.* **1982**, *104*, 4986. (b) Rebek, J. Jr.; *Accts. Chem. Res.* **1984**, *17*, 258. (c) Inouye, M.; Konishi, T.; Isagawa, K. *J. Am. Chem. Soc.* **1993**, *115*, 8091 and references therein.

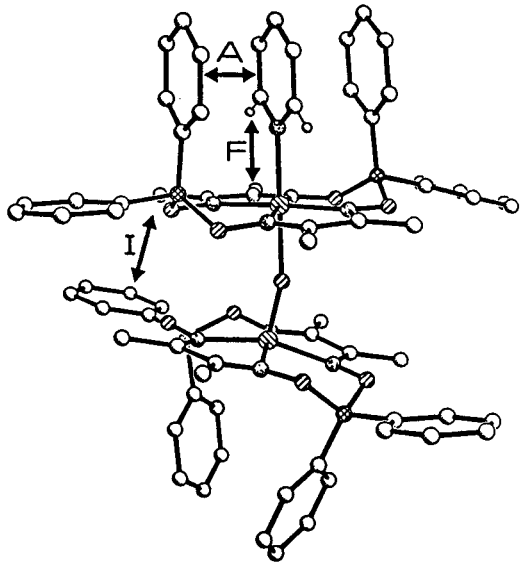

Figure 6. Proposed stereochemical mechanism for the negative cooperativity observed for Py binding to the μ-oxo complex **9**. Axial (A) and facial (F) strain is transmitted to the remote site via interfacial contacts (I). The binding of a second Py requires the opening of the collapsed cavity.

site more (or less) favorable. Allosteric effects typically arise via the propagation of strain energy over large distances via a path of many interconnected nonbonded interactions. The phenomenon is best understood in hemoglobin.[36]

The μ-oxo complexes provide a very simple illustration of negative cooperativity. The stepwise constants for Py and *i*-$PrNH_2$ binding to **9** are as follows: Py, $\log K_1 = 3.8$, $\log K_2 = -0.7$; *i*-$PrNH_2$, $\log K_1 = 3.7$, $\log K_2 = 1.1$.[1g] These amount to reductions in binding free energy at the second site of 6.1 kcal/mol for Py and 3.5 kcal/mol for *i*-$PrNH_2$.

A reasonable stereochemical mechanism for these allosteric effects is given in Figure 6. Face strain and axial contacts within the cyclophane-like cavities surrounding the two binding sites are linked via interfacial contacts between the two FeN_4 units. Interfacial pressures are provided by peripheral groups (phenyls and DMG methyls) on the remote FeN_4 unit. The two N_4 planes lie at van der Waals contact distances in **10**, thus making their interactions extremely sensitive to structural changes on ligation. In a ligated subunit, the peripheral groups project well into the interfacial region where they serve to oppose the corresponding structural changes which must accompany ligation to the second binding site. The allosteric effects in these μ-oxo complexes may also be used to effect heterotropic control of the oxidative reactivity of the μ-oxo group as described elsewhere.[1h]

Acknowledgment. The support of the NSERC Canada is gratefully acknowledged. We thank Javier Matienzo for growing two of the crystals used in this work.

Supporting Information Available: Complete listings of crystallographic details, positional and thermal parameters, and bond lengths and angles, for **3**−**8**, **11**, **12**, and **16**−**20**, a table of nonbonded contacts, and additional ORTEP figures (81 pages). Ordering information is given on any current masthead page.

IC9602761

(36) (a) Baldwin, J.; Chothia, C. *J. Am. Chem. Soc.* **1980**, *102*, 7398.(b) Perutz, M. F. *Annu. Rev. Biochem.* **1979**, *48*, 327. (c) Ho, C. *Annu. Rev. Biochem.* **1992**, *60*, 153.